Combined physical and pharmaceutical anabolic osteoporosis therapies synergistically increase bone response and local mechanoregulation

Authors: Friederike A. Schulte[1†], Julia K. Griesbach[1†], Claudia Weigt, Marcella von Salis-Soglio[1], Floor M. Lambers[1], Francisco C. Marques[1], Michaela Kneissel[3], Peter J. Richards[2,3], Gisela A. Kuhn[1], Ralph Müller[1]*

[1]Institute for Biomechanics, ETH Zurich; Zurich, Switzerland.

[2]Bone and Stem Cell Research Group, CABMM, University of Zurich; Zurich, Switzerland.

[3]Musculoskeletal Disease Area, Novartis Institutes for Biomedical Research; Basel, Switzerland.

[*]Corresponding author. Email: ram@ethz.ch

[†]These authors contributed equally to this work.

Abstract: Despite bone's natural adaptation to mechanical demands, the role of physical therapy alongside osteoporosis drug treatments remains unclear, leaving patients questioning its interaction with medications. Emerging research aims to clarify whether combining physical with drug therapies offers better outcomes for bone strength than either approach alone. Here, we use *in vivo* micro-computed tomography and computational mechanics to investigate the effect of combined physical and drug treatment in a mouse model of osteoporosis. We show that combining mechanical loading with drugs led to synergistically enhanced bone volume, strength, and mechanoregulation in anabolic (parathyroid hormones and sclerostin antibodies) but not in anti-catabolic (bisphosphonate) treatments. At the cellular level, combining drug treatment with mechanical loading shifted (re)modeling thresholds towards higher mechanosensitivity of the cells as described in Frost's mechanostat theory more than 30 years ago. Mechanical loading combined with anabolic treatments shifts formation and resorption saturation levels towards higher, with bisphosphonates towards lower response to mechanical signals. These results underline the potential of combining anabolic drug therapies with physical activity to optimize osteoporosis treatment.

max. 175 (current 171)

Introduction

Postmenopausal osteoporosis is characterized by structural deterioration of bone tissue, leading to increased susceptibility to fractures[1]. Regarding improvements of bone strength, exercise is a cornerstone of bone health, yet its role alongside drug treatments for osteoporosis remains an area of active inquiry. Patients with severe osteoporosis often seek clarity on whether to exercise while on treatment. Many fear that physical activity may interfere with drug efficacy. Others assume that new potent drugs eliminate the need for physical activity. Until recently, little was known about the interplay of physical and drug therapies. Therefore, new evidence is needed as to whether combination therapy can provide better outcomes for bone strength compared to monotherapy.

Amongst current osteoporosis medications, anti-resorptive bisphosphonates inhibit bone resorption by binding to hydroxyapatite crystals in bone, thereby preventing osteoclast attachment and activity, however, their capacity to increase bone mass is low[2]. Newer anabolic parathyroid hormone analogs stimulate bone formation by activation of the osteoblast. The newest anabolic drug, sclerostin antibodies, targets sclerostin, an osteocyte-expressed Wnt-signaling protein[3]. Wnt-signaling is activated by the binding of a Wnt-protein ligand to a Frizzled family receptor on the surface of a cell, which leads to gene transcription inside the cell. By inhibition of a Wnt-signaling antagonist protein, sclerostin antibodies thus promote osteoblast activity while inhibiting osteoclast activity[4]. Sclerostin antibody effects diminish after the first year of treatment in humans, which limits their long-term use as a standalone therapy.

Bone functionally adapts to mechanical demands: highly loaded bones increase their density while disused bones decrease it, a concept referred to as “mechanostat”. It was introduced by Harold Frost[5-7] in the 1980s to explain how bones adjust their structure to maintain a balance between mechanical strength, weight, and metabolic efficiency, building on Wolff's law[8].

According to Frost's theory, bones try to keep their mass constant within a certain load interval and only react to over- or underloads that are defined by mechanical setpoints, similar to a thermostat in which the temperature is kept within a certain temperature range and is only regulated up or down if there is a deviation from the set values. Setpoints in the mechanostat separate the disuse state, where low mechanical strain leads to bone resorption; the adapted state, where balanced strain maintains steady bone mass through a balance of formation and resorption; and the overload state, where increased strain stimulates bone formation, making bones stronger. In the fracture state, excessive strain would lead to microdamage and fractures. Frost's mechanostat theory remains a cornerstone of skeletal biology up to date as it has profound clinical implications. It provides a basis for understanding how physical activity strengthens bones, prevents conditions like osteoporosis, and can help explain how osteoporosis treatments interact with bone’s adaptive responses to mechanical strain. Anti-catabolic bisphosphonates help preserve bone density but prolonged use leads in the case of bisphosphonates to microdamage accumulation and theoretically shifts the setpoints into the pathological fracture state. Anabolic treatments could theoretically push bone formation into the overload window, strengthening bones, provided mechanical loading is also encouraged. According to Frost, combining drug treatments with mechanical loading may offer superior outcomes, as it could enhance the effectiveness of both anabolic and anti-catabolic therapies by promoting bone adaptation in a more dynamic, functional way. Measuring the "setpoints" of osteoporosis medications in the context of Frost's mechanostat theory, however, is not straightforward, as the setpoints themselves are theoretical constructs that describe the mechanical thresholds at which bones adjust their structure, and measuring them experimentally would require complex assessments of both bone volume and mechanical strain under highly controlled conditions.

Biologically, it is known that loads are transferred from the organ to the cellular level eliciting highly coordinated biological responses that result in an adaptation of the internal bone architecture[8]. This process of continuous bone formation and resorption comprises both modeling and remodeling events, collectively referred to as bone (re)modeling[9]. Large portions of the bone (re)modeling can be attributed to osteocyte-induced orchestration of osteoblastic formation and osteoclastic resorption according to local mechanical stimuli[10-13], a concept called 'mechanoregulation'. Portions of site-unspecific non-targeted bone (re)modeling occur, which are, for example, related to maintaining mineral homeostasis[14, 15]. It has been shown that supraphysiological mechanical loading decreases the non-targeted portions of bone (re)modeling[16, 17].

The aim of this study was to explore whether combined drug treatments with mechanical loading leads to improved drug treatment outcomes, i.e. stronger bones. We hypothesized that the combination of drug treatment and mechanical loading shifts the setpoints for bone (re)modeling as proposed by the 'mechanostat' theory more than 30 years ago. We administered bisphosphonate (BIS), parathyroid hormone (PTH), sclerostin antibody (SclAB) or vehicle (VEH) treatment to ovariectomized 20-week-old C57BL/6 mice. Regional sham or mechanical loading (ML) was induced in the sixth caudal vertebra through a highly controlled cyclic mechanical loading model that has previously induced a 20% increase in the trabecular bone volume fraction (BV/TV) of healthy mice[18]. Using this highly controlled system, a combination of animal experiments, time-lapsed *in vivo* micro-computed tomography (micro-CT), and finite-element modeling, we report that mechanical loading in anabolic but not in anti-catabolic osteoporosis therapies synergistically enhanced trabecular bone volume, (re)modeling and mechanoregulation. These findings underscore the potential of physical therapy as an adjunct to anabolic osteoporosis therapies.

Results

Ovariectomy-induced bone loss is reversed by physical and pharmaceutical monotreatments

As described in Fig. 1a, C57BL/6 mice were ovariectomized at 15 weeks-of-age. Bone loss was confirmed in all animals (n=105) by *in vivo* micro-CT of the 6th caudal vertebra (-26.8±9.7% change in BV/TV compared to before surgery, data presented as mean ± standard deviation). From week 20 to 24, animals received pharmaceutical treatment and/or mechanical loading. The VEH-group showed a further decrease in BV/TV between weeks 20 and 24 (-10.1±7.6%, Fig. 1b). In all monotreatment groups including the ML-group, BV/TV increased (ML: 17.7±11.0%; BIS: 14.4±8.5%; PTH: 22.1±10.0%; SclAB: 25.3±12.7%; Fig. 1b). The BIS-group showed no significant increase in trabecular thickness (Tb.Th: 4.8±4.0%) compared to the VEH-group (0.5±4.4%). The anabolic treatment groups increased in Tb.Th with the increase in the PTH-group being significantly less pronounced than the other anabolic treatment groups (ML: 20.6±8.3%, PTH: 11.6±4.7%, SclAB: 25.3±6.9%; Fig. 1c). Trabecular number (Tb.N) was preserved in the BIS-group (1.1±2.9%), and decreased in all other groups (VEH: -8.8±4.0%; ML: -8.1±3.4%; PTH: -6.3±2.9%; SclAB:-10.4±2.7%; Fig. 1d). Connectivity density (Conn.D) was preserved in the BIS-group (1.1±15.3%) and the PTH-group (PTH: -6.4±20.5%) and decreased in all other groups (VEH: -21.2±11.2%; ML: -29.5±12.9%; SclAB: -35.0±8.3%; Fig. 1e).

Figure 1f shows bone formation and resorption volumes evolving over time. Bone formation rate (BFR) in week 22 to 24 in the BIS-group (BIS: 1.0±0.2%/d) was lower than in the PTH- and SclAB-group (PTH: 1.5±0.3%/d, SclAB: 1.6±0.3%/d, Fig. 1g), with no significant differences to VEH or ML (VEH: 1.3±0.5%/d; ML: 1.4±0.3%/d). Mineral apposition rate (MAR) did not differ significantly amongst groups (Fig. 1h). Mineralizing surface (MS) was higher in the anabolic groups (ML: 56.5±6.8%, PTH: 63.3±4.0%, SclAB: 68.0±5.6%, Fig. 1i)

than the VEH- and BIS-groups (VEH: 41.2±6.3%, BIS: 42.4%±3.3, Fig. 1i). Bone resorption rate (BRR) was significantly reduced in all treatment groups (BIS: 0.6±0.2%/d; ML: 0.7±0.2%/d; PTH: 0.5±0.2%/d; SclAB: 0.5±0.2%/d; Fig. 1j) compared to the VEH-group (VEH: 1.4±0.3%/d). Mineral resorption rate (MRR) was significantly lower in the BIS-group (BIS: 1.1±0.1µm/d) than in the VEH-group (1.7±0.2µm/d), being unchanged in the anabolic treatment groups (ML: 1.7±0.3µm/d; PTH: 1.6±0.1µm/d; SclAB: 1.7±0.2µm/d; Fig. 1k). This can explain why bisphosphonate treatment preserves Tb.N because no full trabeculae are resorbed. Eroded surface (ES) was significantly reduced in the anabolic treatment groups (ML: 22.0±4.6%; PTH: 19.5±3.2%; SclAB: 14.0±3.3%; Fig. 1l), compared to VEH or BIS (VEH: 30.6±4.9%; BIS: 29.5±3.9%;).

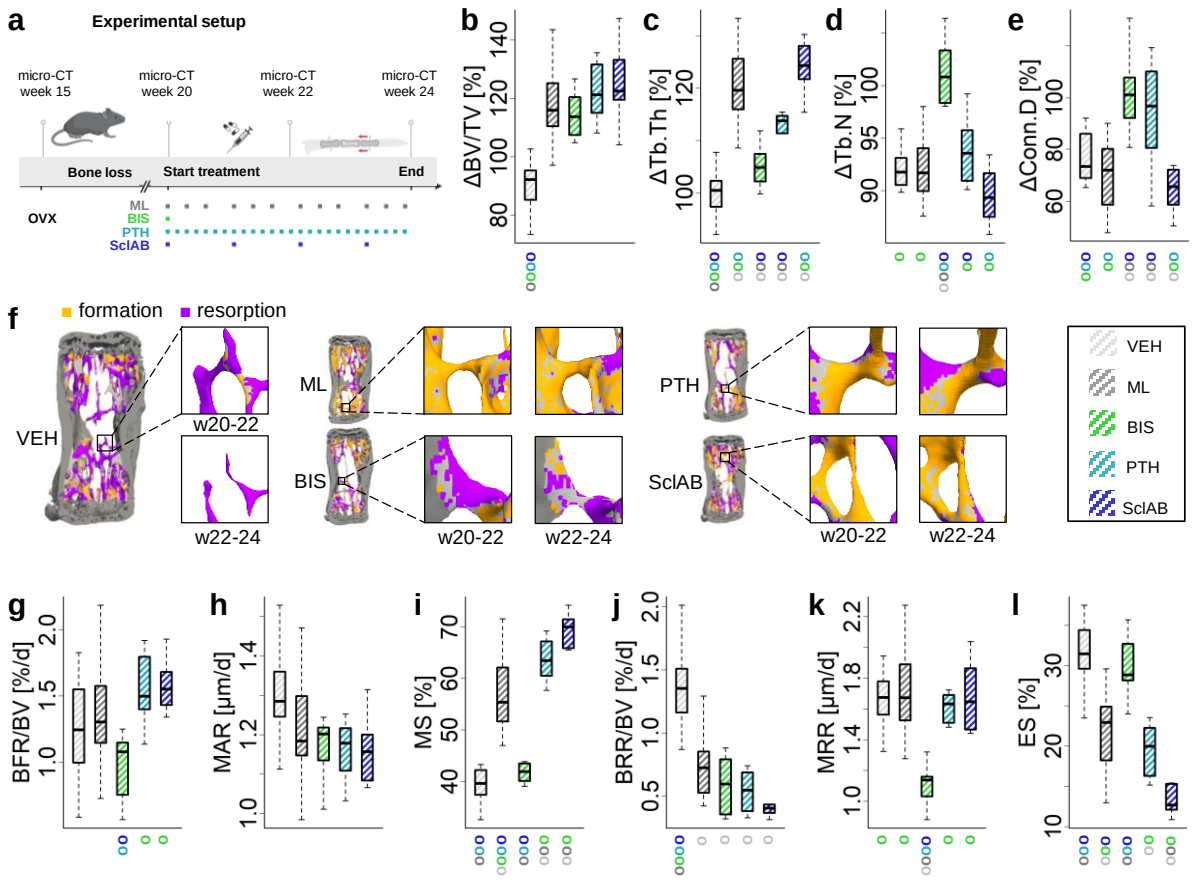

Figure 1: Osteoporosis monotreatments enhance trabecular bone micro-architecture by different mechanisms of action. *(**a**) Experimental setup. 15-week-old mice are ovariectomized and treatment is administered between week 20 (w20) and 24 (w24). Created with Biorender (**b-e**) Monotreatments (VEH: n=29, BIS: n=9, PTH: n=10, SclAB: n=9), boxplots show percentage change over four weeks in (**b**) bone volume fraction ΔBV/TV, (**c**) trabecular thickness ΔTb.Th, (**d**) trabecular number ΔTb.N (**e**) connectivity density ΔConn.D (**f**) representative micro-computed tomography overlays at intervals w20-w22 and w22-w24, with (re)modeling volumes (**g-l**) (Re)modeling rates calculated from time interval w22-w24 (**g**) bone formation rate BFR (**h**) mineral apposition rate MAR (**i**) mineralizing surface MS (**j**) bone resorption rate BRR (**k**) mineral resorption rate MRR (**l**) eroded surface ES. The symbol '**o**' denotes p<0.05 using ANOVA with Tukey post-hoc test (to VEH: light grey; to ML: dark grey; to BIS: green; to PTH: cyan; to SclAB: blue).*

Mechanical loading synergistically affects trabecular bone volume and mechanical performance in anabolic treatments

Next, we investigated to which extent additional mechanical loading further enhanced the morphological changes and mechanical integrity in response to pharmaceutical treatment. BV/TV in the BIS + ML-group increased 28.0±4.4% (Fig. 2a, Table 1) but neither exceeded the sum of the single treatment responses nor was statistically significantly different from the BIS-group. The increase in BV/TV in the anabolic treatment groups exceeded the sum of the monotreatment responses (PTH + ML: 46.3±16.8%, SclAB + ML: 59.4±21.1%), indicating synergistic behaviour. ΔTb.Th in the BIS + ML group (19.3±2.5%; Fig. 2b) was significantly higher than in the BIS group, to an extent comparable to the ML-group. Tb.Th in PTH + ML and SclAB + ML was significantly higher than in the PTH-group and SclAB-group after four weeks, and was considered additive (PTH + ML: 33.3±11.3%; SclAB + ML: 49.9±19.4%). ΔTb.N was preserved in the BIS + ML group, even with additional mechanical loading (-1.4±2.2%; Fig. 2c). Interestingly, ML as a monotreatment had reduced Tb.N, and this effect was blunted by additional BIS treatment. The loss of Tb.N observed in SclAB could not be reversed in SclAB + ML (-8.3±1.8%). Conn.D as a measure of the structural integrity and interconnectedness of the trabecular network, was preserved the most in BIS + ML, and PTH

+ ML (BIS + ML: -17.8±8.0%; PTH + ML: -29.0±11.0%; SclAB + ML: -45.4±7.8%; Fig. 2d). Cortical area fraction (Ct.Ar/T.Ar; BIS + ML: 7.8±1.4%; PTH + ML: 19.3±5.0%; SclAB + ML: 25.8±5.2%; Fig. 2e) and cortical thickness (Ct.Th; BIS + ML: 3.4±0.9%; PTH + ML: 6.5±3.8%; SclAB + ML: 17.1±4.1%; Fig. 2f) showed synergistic behaviour in both anabolic treatment groups PTH + ML and SclAB + ML.

To investigate if increases in BV/TV were associated with increased trabecular strength thus giving indication of decreased fracture risk, we assessed mechanical performance parameters of resulting structures over four weeks. Trabecular strength increased in all treatment groups, with loading-induced increases being additive in the PTH + ML group and synergistic in the SclAB + ML group (BIS + ML: 42.4±5.7%; PTH + ML: 70.6±21.4%; SclAB + ML: 95.2±36.4%; Fig. 2g). Mean and maximum strain energy density (SED) decreased in all treatment groups, being most pronounced in the combination groups, but revealed only interfering decreases (SED: BIS + ML: -43.3±3.3%; PTH + ML: -54.4±8.5%; SclAB + ML: -62.8±9.0%; Fig. 2h,i, Table 2). Linear regression analysis showed that the changes in trabecular strength correlated highly with the changes in BV/TV and Tb.Th (BV/TV: R^2 = 0.86, Tb.Th: R^2 = 0.74, Fig. 2k).

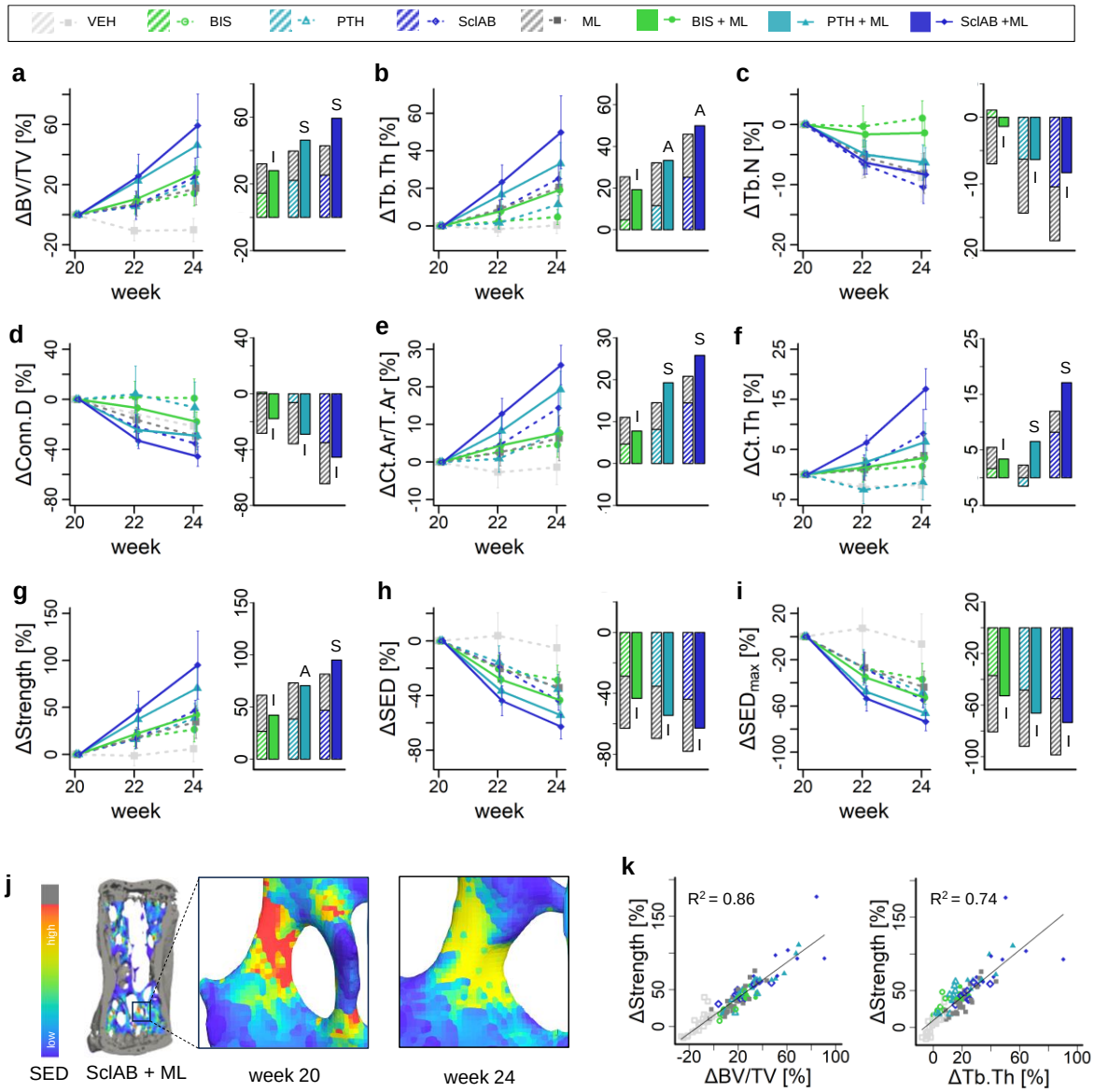

Figure 2: Mechanical loading increases the morphological parameters of anabolic and anti-catabolic pharmaceutical treatments, which contribute to increased strength. *Change in parameter in % compared to week 20; sum of single vs. combined treatment indicating graphically interfering (I), additive (A) or synergistic (S) effects* ***(a)*** *bone volume fraction (ΔBV/TV)* ***(b)*** *trabecular thickness (ΔTb.Th)* ***(c)*** *trabecular number (ΔTb.N)* ***(d)*** *connectivity density (ΔConn.D)* ***(e)*** *cortical bone volume fraction (ΔCt.BV/TV)* ***(f)*** *cortical thickness (Ct.Th)* ***(g)*** *ΔStrength, and* ***(h)*** *ΔSED* ***(i)*** *ΔSEDmax* ***(j)*** *Representative image of the strain-energy density (SED) distribution in the 6th caudal vertebra of a SclAB + ML animal and a zoom-in on a trabecular detail at week 20 and week 24, showing a heterogeneous site of high SED (week 20) and a structural reorganization resulting in a reduction in SED (week 24).* ***(k)*** *Linear regression analysis of ΔStrength with ΔBV/TV, and Δtrabecular thickness (ΔTb.Th) in week interval 20-24.*

Table 1: Significance levels of static morphometric and mechanical parameters as difference from end of treatment at week 24 to start of treatment at week 20. *Significances were calculated using ANOVA with Tukey post-hoc test; significant*

*differences are depicted with a symbol in the color of the corresponding group (**o**: to monotreatment, ●: to combined treatment, $p<0.05$).*

Parameter	VEH	ML	BIS	BIS + ML	PTH	PTH + ML	SclAB	SclAB + ML
ΔBV/TV [%]	oooo ●●●	o ●●	o ●●	o ●●	o ●●	ooooo ●	o ●●	ooooo ●
ΔTb.Th [%]	ooo ●●●	ooo ●●	oo ●●●	ooo ●●	ooo ●●●	ooooo ●●	ooo ●●	ooooo ●●
ΔTb.N [%]	o ●	o ●	oooo ●●	oooo ●●	o ●	o ●	o ●	o ●
ΔConn.D [%]	ooo ●	oo ●	ooo ●●●	oo ●●	ooo ●●	oo ●	oooo ●	oooo ●
ΔCt.BV/TV [%]	oooo ●●●	oo ●●	oo ●●	o ●●	oo ●●	oooo ●●	oooo ●	ooooo ●●
ΔCt.Th [%]	ooo ●●●	oo ●	ooo ●●	oo ●	ooo ●●●	ooo ●	ooo ●	ooooo ●●
ΔCt.BS/TV [%]	oo ●●	o ●●	oo ●	ooo ●	oooo ●●●	ooooo ●●	o ●	o ●
ΔSED [%]	oo ●●●	o ●		o ●		oooo	o ●	ooooo ●
ΔmaxSED [%]	oooo ●●●	o ●●	o ●●	o ●●	o ●●	ooooo ●	o ●●	ooooo ●
Δeff [%]	oooo ●●●	o ●●	o ●●	o ●	o ●●	ooooo	o ●●	ooooo ●
ΔStrength [%]	oooo ●●●	o ●●	o ●●	o ●	o ●	ooo ●	o ●	ooooo ●●

Mechanical loading synergistically increases bone formation rates and suppresses bone resorption rates in anabolic treatments

Bone formation rate (BFR) in the anabolic combination groups exceeded the sum of the monotreatment responses (Fig. 3a). MAR showed synergistic behaviour in all combination groups. It was lowered in the SclAB-group and increased in the SclAB + ML-group (Fig. 3b). MS in BIS + ML showed beneficial increases, in PTH + ML and SclAB + ML additive increases (Fig. 3c). Synergisms in the BFR of anabolic treatments seemed thus only explainable through the increases in MAR. Bone resorption rate (BRR) was reduced in all treatment groups (Fig. 3d) but in the BIS + ML-group, the observed reduction in BRR by BIS treatment was marginally altered by mechanical loading. The anabolic treatment groups showed additive (PTH+ML) and interfering (SclAB + ML) decreases in BRR (Fig. 3d). The BIS + ML group was characterized by decreases in MRR, which were not altered by mechanical loading (Fig. 3e). MRR was

synergistically reduced in the PTH + ML group and additively reduced in the SclAB + ML-group. Synergistic decreases in ES were observed for PTH + ML and SclAB + ML (Fig. 3f). Trabecular microstructures and representative inlets of the combination groups are depicted in Fig. 3g. Changes in strength were correlated linearly with BFR and decayed exponentially with BRR, indicating that small reductions of the bone resorption rate under treatment can result in large increases in trabecular strength.

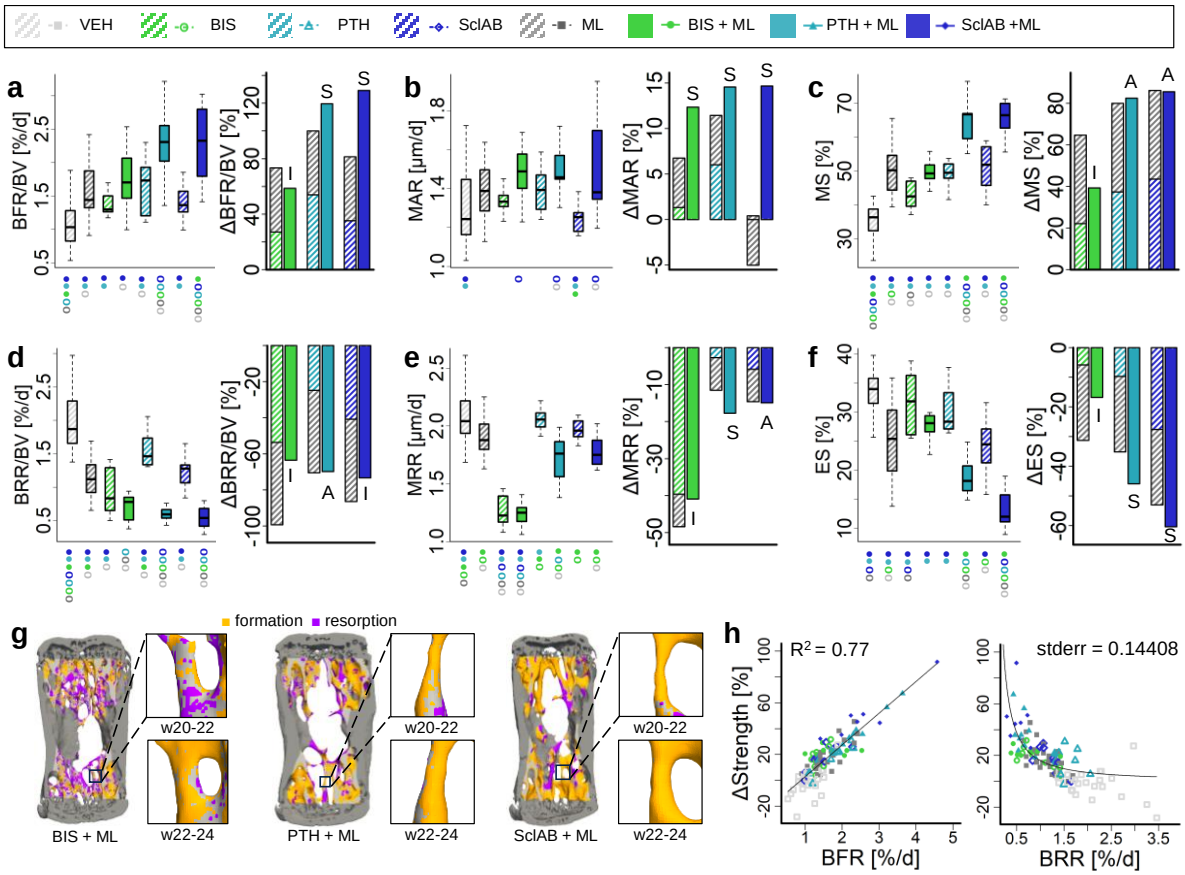

***Figure 3**: Mechanical loading increases bone formation and decreases resorption rates of anabolic and anti-catabolic pharmaceutical treatments which contribute to increased strength.* *Δ denotes change from VEH as no baseline value for dynamic bone morphometry rates was available; sum of single vs. combined treatment indicating graphically antagonistic (I), additive (A) or synergistic (S) effects (**a**) bone formation rate per bone volume (BFR/BV) (**b**) mineral apposition rate (MAR) (**c**) mineralizing surface (MS) (**d**) bone resorption rate per bone volume (BRR/BV) (**e**) mineral resorption rate (MRR) (**f**) eroded surface (ES). Significances were calculated using ANOVA with Tukey post-hoc test; significant differences are depicted with a symbol in the color of the corresponding group (**o**: to monotreatment, ●: to combined treatment, $p<0.05$). (**g**) Visual representations of combination groups BIS + ML, PTH + ML, and SclAB + ML in time intervals week (w) 20-22 and 22-24 (**h**) Linear regression analysis in intervals 20-22 of ΔStrength with bone formation rate (BFR), and exponential regression analysis with bone resorption rate (BRR).*

Bone formation and resorption occur in mechanically distinct ranges

To address the question whether pharmaceutical treatments target bone (re)modeling to the places that mechanically need it, we correlated the underlying mechanical signals in the trabecular compartment with subsequent formation and resorption events. Visually, spatial agreement between sites of high SED and regions of subsequent bone formation, intermediate strains and sites of quiescence, and low strains and sites of subsequent bone resorption were found (Fig. 4). Quantitatively, mean SED at formation, quiescent and resorption sites expressed as percent difference from the mean (over all animals) quiescent SED, showed significantly higher mean SED in formed than in quiescent, and significantly lower SED-values in resorbed than in quiescent surfaces. The addition of mechanical loading to the monotreatments resulted in marginal changes of this apparent natural law, indicating that bone formation and resorption occur in mechanically distinct ranges despite possible influences of pharmaceutical interventions. It could, however, be that the natural law is that strong that it masks subtle differences between treatments.

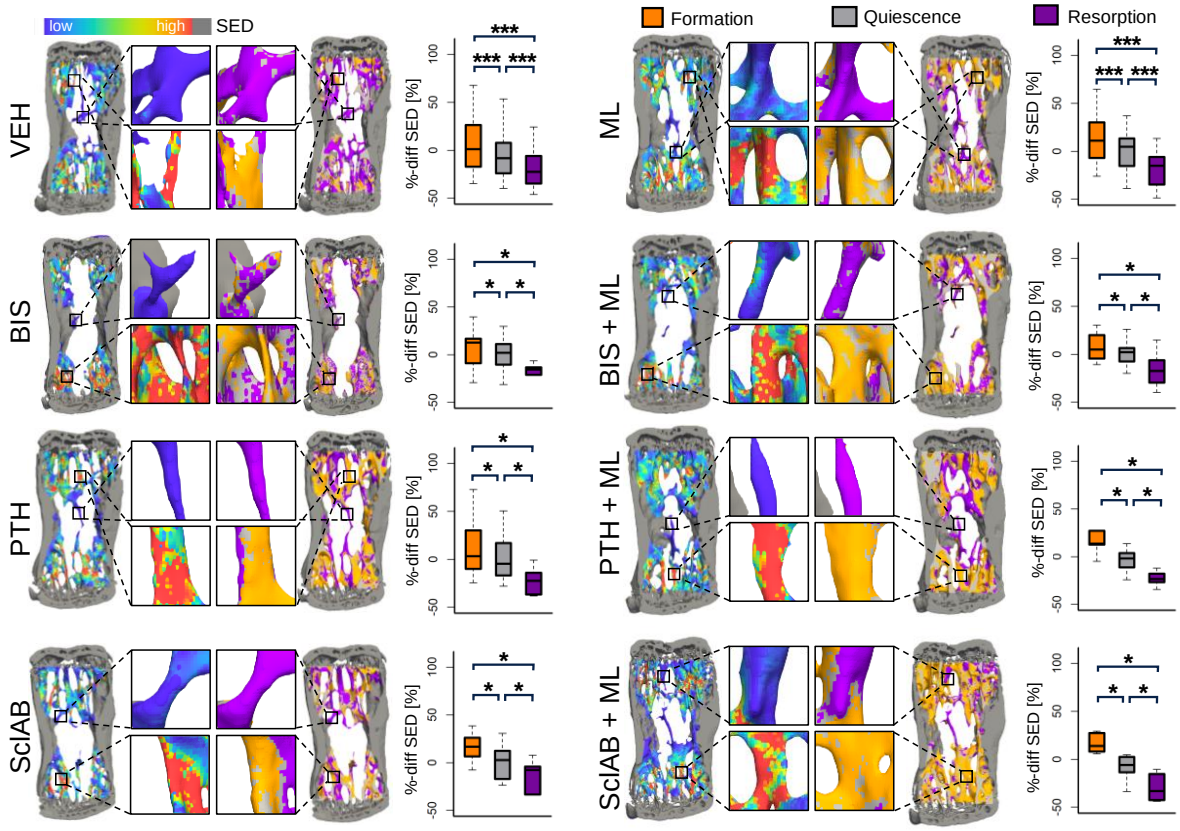

Figure 4: Formation occurs at high mechanical signal and resorption at low mechanical signal*: Visual three-dimensional mechanical environment (SED computed with micro-finite element analysis in the basal scan at week 20) compared to trabecular bone formation and resorption volumes over 2 weeks (week 22). Relative difference to mean quiescent SED in formed, resorbed, and quiescent sites[10]. *p<0.05, ***<0.001 using paired Wilcoxon-test, with Bonferroni correction.*

Dependence of (re)modeling probability on mechanical stimulus

Next, we investigated whether the direct dependence of formation and resorption volumes on mechanical signals is influenced by drug administration. Conditional probabilities of (re)modeling events formation, quiescence, resorption for a given SED-value were calculated and the resulting curves were fitted with exponential functions. The probability for bone formation increased with increasing SED, and the probability for bone resorption decreased with increasing SED (Fig. 5a-d). Mechanoregulation was more pronounced in ML compared to VEH, visible in the extremes starting lower for low mechanical strain and ending higher for high mechanical strain (Fig. 5a). BIS and BIS + ML showed lower slopes than VEH, confirming

decreased bone turnover shown by dynamic bone morphometry (Fig. 5b). PTH and PTH + ML curves opened up, indicating a higher turnover and responsiveness to mechanical signals, indicated by steeper slopes than VEH (Fig. 5c). In SclAB and SclAB + ML, the formation and resorption curves resembled the ML curve and were shifted up and down respectively, while the slopes were not affected, meaning SclAB + ML fostering the readiness of the cells for formation, indicating an increase in the osteocyte mechanosensitivity, which also explains the dual-action mode (Fig. 5d).

The area under the curve for the receiver operating characteristic for formation (AUC_F) and resorption (AUC_R) are descriptors for (re)modeling-specific mechanoregulation. Combined anabolic treatments resulted in increased mechanoregulation of bone formation with AUC_F values of 0.697 (PTH+ML) and 0.711 (SclAB+ML) compared to VEH (0.615), ML (0.631), BIS (0.573) and BIS + ML (0.585). BIS and BIS + ML resulted in significantly lower AUC_F values than the other groups. Mechanoregulation of bone resorption, reflected in AUC_R, was increased in ML (0.525), SclAB (0.531), BIS + ML (0.529), PTH + ML (0.555) and SclAB + ML (0.558) compared to VEH (0.513; Fig. 5g). BIS (0.517) and PTH (0.526) had no significant effect on AUC_R compared to VEH.

In ML, non-targeted formation (VEH: 0.247, ML: 0.237; Fig. 5i) and resorption (VEH: 0.245, ML: 0.21; Fig. 5i,j) were decreased. In BIS, non-targeted formation was increased compared to VEH (0.258) and BIS + ML was the highest amongst all groups (BIS + ML: 0.268). PTH decreased non-targeted formation (0.242), the effects were less than in ML (0.237), and the effects on non-targeted resorption (0.211) were similar to ML. The PTH + ML group showed the lowest fraction of non-targeted formation (0.224) and resorption (0.181) among the investigated therapies. SclAB decreased non-targeted formation (0.232) more than ML or PTH. It decreased non-targeted resorption (0.235), but less than ML or PTH. SclAB + ML increased

non-targeted formation (0.238) and decreased non-targeted resorption (0.218) compared to SclAB.

BIS + ML had the lowest resorption/quiescent intersection value (RQ, Fig. 5k), meaning there was only a small range of mechanical values where resorption probability was higher than quiescence or formation. PTH + ML had the highest intersection value RQ, where resorption was most likely to occur for the biggest SED range. BIS and BIS + ML decreased RQ compared to VEH. Only minor changes were observed in the quiescence/formation intersection value (QF, Fig. 5l). SclAB + ML was the only treatment that decreased QF compared to VEH, meaning formation probability was dominant over the largest SED range among all treatments.

Fig. 6 illustrates the SED-distribution in trabecular bone changing over time. In several areas in VEH, high SED values decreased over time, but in other areas they increased. Additionally, Fig. 6 illustrates how the resorption of a single trabecula leads to a more heterogeneous SED distribution. While SED on average decreased over time for BIS + ML, this did not particularly affect areas with high SED, as there remained several highly strained areas in week 24. In contrast, both PTH + ML and SclAB + ML showed large decreases in SED, especially in areas with high SED values in week 20.

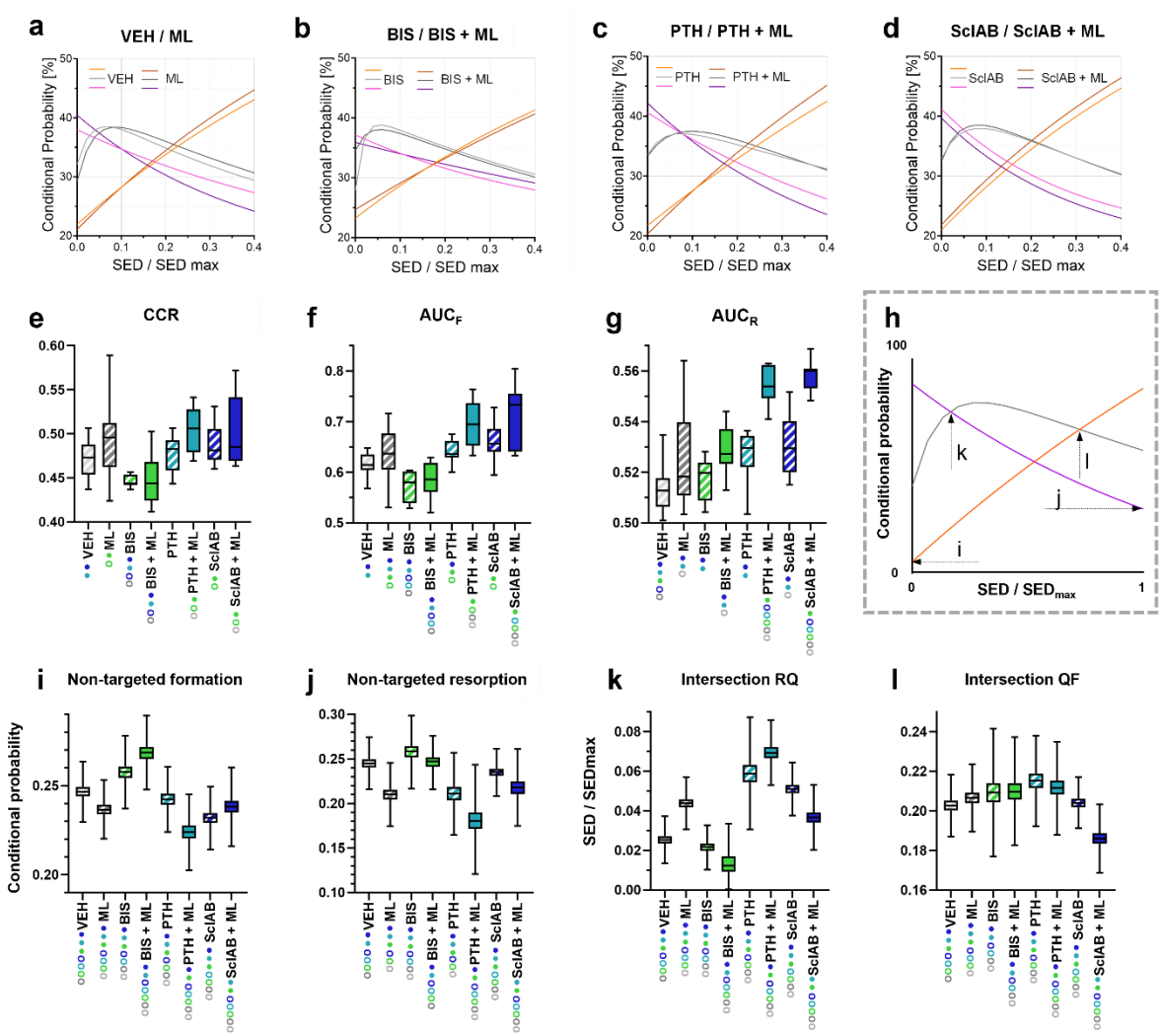

Figure 5: Conditional probabilities and quantification of mechanoregulation show differences between treatments. (a-d) *conditional probability curves,* ***(e)*** *CCR,* ***(f)*** *AUC formation,* ***(g)*** *AUC resorption* ***(i-l)*** *points of interest from conditional probability curves, which are explained in* ***(h)*** *an example conditional probability curve. Significances were calculated with one-way Anova or Kruskal-Wallis based on normality with Tukey post-hoc-test and significant differences are depicted with a symbol in the color of the corresponding group (**o**: to monotreatment, ●: to combined treatment, p<0.05).*

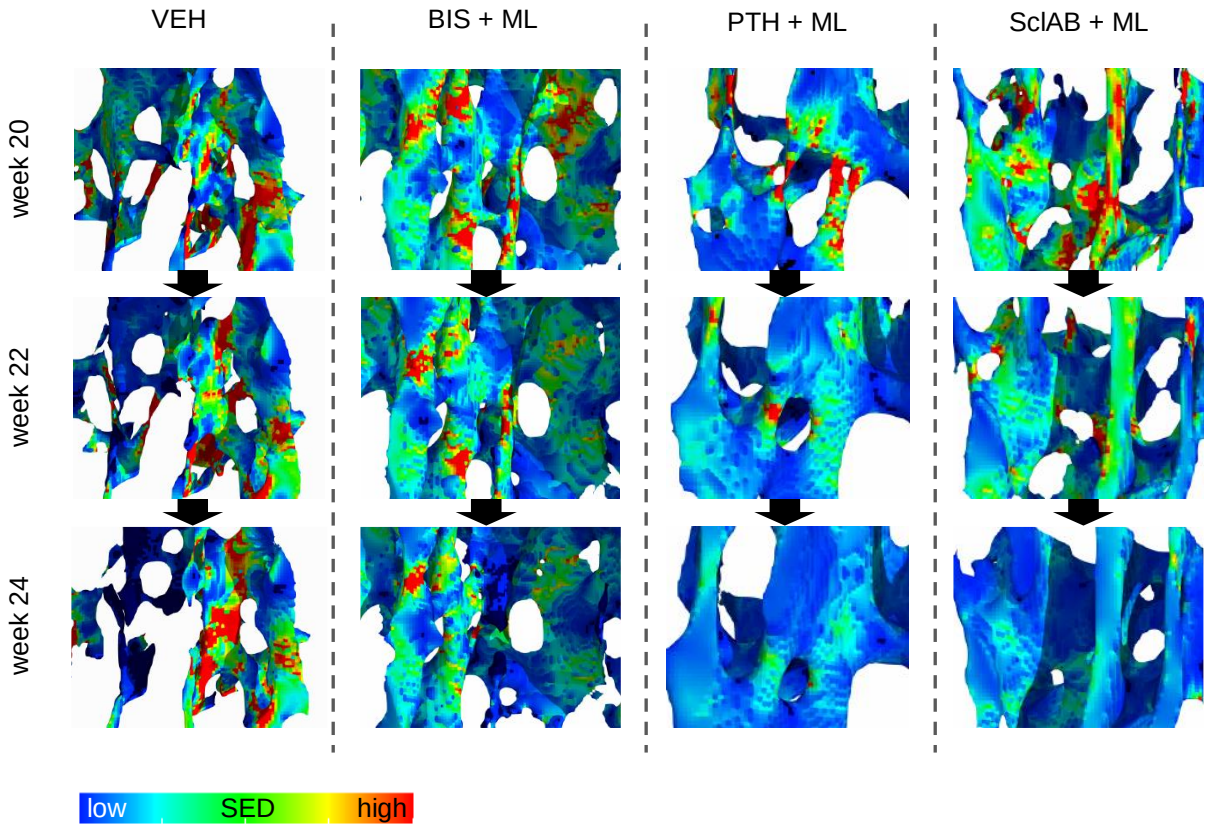

***Figure** 6**: Heterogeneity of the strain distribution decreases to different extents in different treatments.** Qualitative comparison of changing SED-distribution for VEH, BIS + ML, PTH + ML and SclAB + ML over the course of 4 weeks of treatment.*

Synergisms in (re)modeling velocity and mechanostat parameters

To assess potential shifts in the setpoints due to different drug or combination treatments, mean (re)modeling velocity (RmV) curves and mechanostat parameters[16] were calculated for each treatment group as an approximation to the mechanostat theory. These curves show the net RmV for a given surface effective strain, where a negative value means net resorption and a positive value means net formation. Minimum and maximum RmV, as well as (re)modeling thresholds (RmTs) were extracted from the resulting curve. Treatment increased RmV (Fig. 7a-d), minimum and maximum RmV (Fig. 7i,j), as well as decreased the RmT for all groups but PTH + ML (Fig. 7k) compared to VEH. PTH + ML did not have an RmT as it increased the RmV especially for low strains, leading to net bone formation across the whole range of

effective strains. Combined treatments generally led to higher RmVs than monotreatments, except for BIS + ML. Using VEH as the control, the RmV curve from ML was shifted up along the y-axis with a slight decrease in curvature (Fig. 7a). BIS caused a RmV curve with a steep increase at low effective strain, after which the curve abruptly bent into an almost linear function with a low gradient. This effect was even more pronounced in BIS + ML. PTH increased RmV overall and decreased the curvature of the function compared to VEH/ML. PTH + ML led to an almost linear curve, except for a small increase for low effective strain. SclAB and SclAB + ML led to similar RmV curves or ML and were only shifted up along the y-axis.

To analyze potential synergies , we calculated the differences between each treatment-induced RmV-curve and the VEH RmV-curve. We provided the treatment effects of the respective monotreatments, the effect of the combined treatment, and the theoretical effect of adding both monotreatment effects. BIS + ML showed an interfering effect on RmV (Fig. 7f) . Fig. 7g shows that the combined treatment was consistently higher than both monotreatment effects, indicating synergy, with the effect of PTH + ML treatment greatest for very low effective strains. SclAB monotreatments effects were higher than those of ML, and SclAB + ML combined caused a greater effect than the addition of the effects of the monotreatments, indicating synergism, except for <0.0001 effective strain (Fig. 7h). In contrast to PTH + ML, SclAB + ML caused a more consistent increase across all effective strain levels, as suspected by the similar shape of the SclAB + ML RmV curve compared to VEH.

The analysis of the minimum RmV, i.e. resorption saturation level RSL, (Fig. 7i) showed that BIS + ML decreased it (-0.00585 µm/d) as compared to the respective monotreatments (BIS: -0.00169 µm/d; ML: -0.00343 µm/d), while it was increased by the other combined treatments as compared to their respective monotreatments. VEH (-0.00837 µm/d) resulted in the lowest and PTH + ML (0.00301 µm/d) in the highest minimum RmV, i.e. formation saturation level FSL which was highest for SclAB + ML (0.00721 µm/d), even when compared to PTH + ML

(0.00676 µm/d; Fig. 7j). BIS + ML (25.0 µε) resulted in the lowest RmT, followed by SclAB + ML (35.0 µε) and BIS (70.0 µε; except PTH + ML), while VEH resulted in the highest RmT (1050.0 µε) (Fig. 7k).

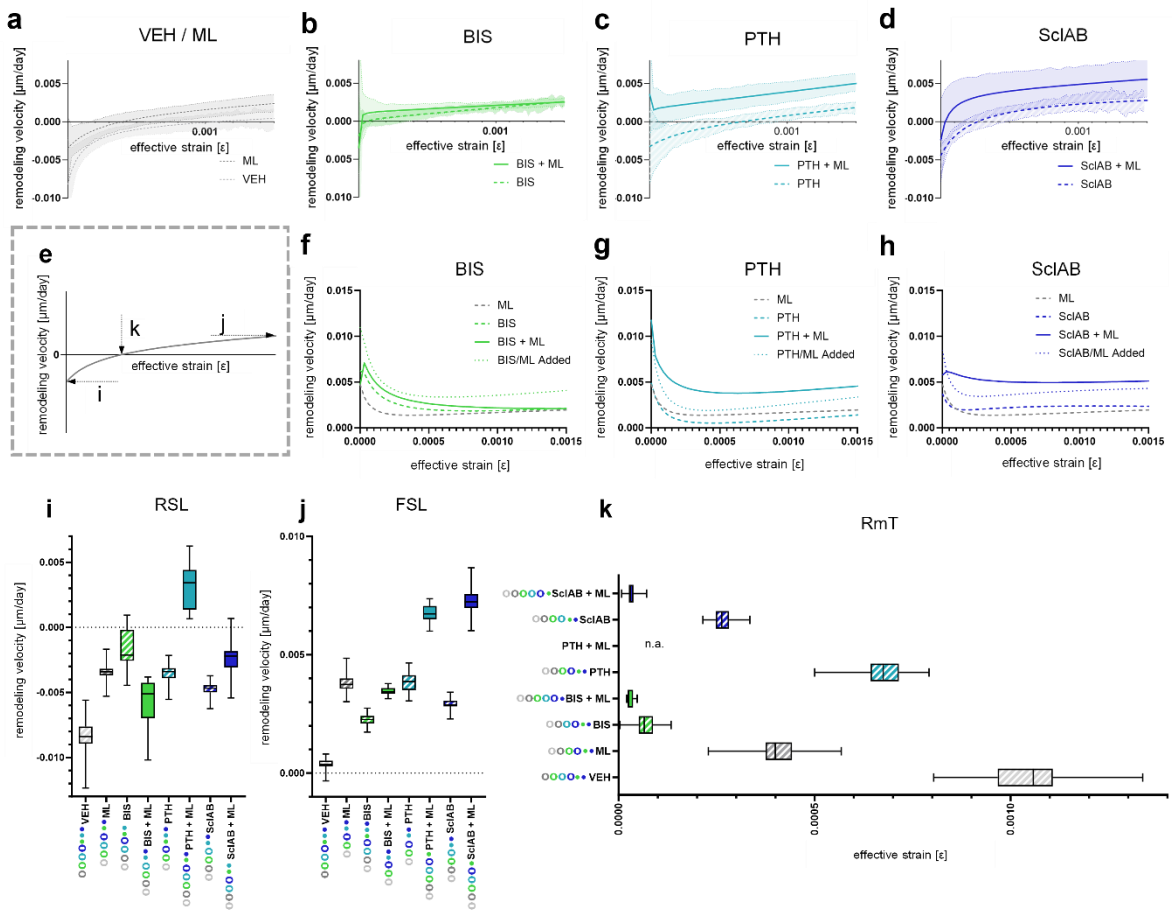

Figure 7: (Re)modeling velocity curves are altered by mono- and combined treatments. (a-d) *(re)modeling velocity (RmV) curves for* ***(a)*** *VEH / ML,* ***(b)*** *BIS / BIS + ML,* ***(c)*** *PTH / PTH + ML,* ***(d)*** *SclAB / SclAB + ML;* ***(e)*** *example RmV curve explaining the extracted parameters in i,j and k* ***(f-h)****: treatment effects on the RmV curves comparing the effects of combined treatments with the respective monotreatments they consist of* ***(f)*** *BIS / BIS + ML,* ***(g)*** *PTH / PTH + ML,* ***(h)*** *SclAB / SclAB + ML.* ***(i)*** *resorption saturation level (RSL),* ***(j)*** *formation saturation level (FSL) and* ***(k)*** *(re)modeling threshold (RmT) of the (re)modeling velocity curves. Significances were calculated with Kruskal-Wallis test and Tukey post-hoc test; significant differences are depicted with a symbol in the color of the corresponding group (****o****: to monotreatment, ●: to combined treatment, p<0.05).*

Discussion

The main goal of osteoporosis therapy is to prevent fractures. To do this efficiently, bone has to be maintained and newly built at mechanically relevant sites. In healthy bone, this is regulated via the mechanostat. Here, we investigated how drug treatments influence this regulation and whether drug performance can be improved by mechanical loading. Our findings suggest that current osteoporosis drugs build bone (anabolic) and inhibit bone resorption (anti-catabolic) at the mechanically relevant sites. Combining physical with anabolic but not anti-catabolic osteoporosis treatments leads to a synergistic trabecular bone response and local mechanoregulation compared to the respective monotreatments. PTH and SclAB treatment benefitted from mechanical loading, indicated by synergistic bone response including increased mechanosensitivity compared to monotreatment. Although bisphosphonate treatment was not impaired by combination with mechanical loading, the deleterious effects of bisphosphonates on mechanoregulation could not be recovered.

In the current study, sclerostin antibody treatment resulted in a synergistic increase in bone volume fraction, strength, and (re)modeling velocities when combined with mechanical loading. Bone formation rate was increased, and bone resorption rate was decreased as compared to single treatments, being in line with previous publications[4, 19, 20]. Morse and colleagues showed that the combination of mechanical loading with sclerostin antibodies in healthy young mouse tibia led in cortical but not trabecular bone to a synergistic bone response[21]. In the FRAME clinical trial, it was found that bone-forming effects of Romosozumab, a clinical version of sclerostin antibodies, on periosteal surfaces may require mechanical loading and potentially only manifest themselves in weight-bearing sites[22]. Morse et al.[21] reported sclerostin antibody treatment combined with mechanical loading affected different genes related to the Wnt/β-catenin pathway, which could be a reason for a synergistic response elicited. SOST -/-knockout mice showed a bone response to mechanical loading, thus

other proteins than sclerostin are involved in the bone response to loading[23]. One candidate could be the Dickkopf-1 (Dkk1) protein which when inhibited in combination with sclerostin, resulted in a robust osteoanabolic effect in mice[24]. Dual inhibition of DKK1 and sclerostin led to a synergistic formation of bone[24-26]. Choi et al.[27] reported, in response to mechanical loading, histone deacetylase5 (HDAC5) suppresses myocyte enhancer factor2 (MEF2), which reduced the expression of SOST and DKK1 levels[28, 29]. Robling et al.[30] showed that mechanical loading reduced SOST mRNA by 73% and Dkk1 transcripts by 49%. This inhibition may occur at the LRP5/6 receptor on osteocytes and osteoblasts, which is the receptor involved in the Wnt/β-catenin pathway where Wnt, sclerostin, and DKK1 proteins compete for binding. The receptor's 46-bladed propellers have distinct binding sites: Wnt1, Wnt2, Wnt6, Wnt7a/b, Wnt9a/b, Wnt10a/b, DKK1, WISE, and SOST bind to the first propeller, while Wnt3, Wnt3a, and DKK1 bind to the third[31]. Inhibition of Wnt inhibitors at the LRP5/6 receptor through mechanical loading (SOST, DKK-1) and sclerostin antibodies (SOST) could potentially explain the synergistic bone response of sclerostin antibodies and mechanical loading.

We found increased sensitivity of mechanoregulation mechanisms for PTH + ML but not for only PTH compared to VEH (Fig. 7), which is in line with the results of Ryder et al.[32], where PTH combined with fluid flow increased the mechanoresponse of osteoblasts, although PTH alone did not. Hagino et al.[33] hypothesized that PTH lowers the (re)modeling threshold of the (re)modeling velocity function, which our findings support (Fig. 7). Notably, combining PTH with mechanical loading lowered the (re)modeling threshold to such an extent that the entire (re)modeling velocity curve was positive, meaning that even for very low effective strain, there is more formation than resorption, leading to net bone formation. These results are in agreement with data from studies by Miller et al.[34], where the effects of PTH + ML resulted in an overall increase of cortical thickness at zero longitudinal strain, and effects varied for different surface strains. In previous animal studies, mechanical loading combined with intermittent PTH (1-34)

led to synergistic effects in cortical but not trabecular bone of the proximal tibia and distal ulna in 13-17-week-old healthy mice[35]. The missing synergistic trabecular effects of loading might have been obscured by the dramatic dose-related effects that PTH alone had on trabecular bone. In 19-month-old healthy mice, additive benefits in the periosteal cortical regions of the tibia were reported at 50 μg/kg/day intermittent PTH while in the trabecular bone the loading-related increase in BV/TV was abrogated[36]. Robinson et al. reported synergistic effects in the trabecular compartment of the healthy tibia, but only prevalent in regions that were not remodeled but modeled [37].

In our study, bisphosphonates were the only treatment that preserved Tb.N compared to all other groups. Clinical studies on postmenopausal women found no effects of combination treatment[38], with differences of bisphosphonate treatment alone depending on the bone and site[39], while Kistler-Fischbacher et al.[40] found positive effects of bisphosphonate and mechanical loading treatment in the load-bearing femoral neck which were less pronounced in the spine, and also dependent on the kind of exercise. Stadelmann et al. [41] found additive effects on cortical thickness for several areas, however, bisphosphonates seemed to impair mechanical loading in regions of high strains, which suggested altered mechanosensation. Sugiyama et al.[42] found no improvements of combining bisphosphonates and mechanical loading in trabecular C57BL/6 mouse tibial bone. This corroborates our finding of decreased mechanoregulation under bisphosphonate treatment (Fig. 5j), which could not be recovered by additional mechanical loading and showed that bisphosphonates decreased bone formation where it was mechanically most needed (Fig. 7j). Since mineralizing and eroded surfaces were similar in the bisphosphonate group compared to the vehicle group, our results suggest that bisphosphonates not only affect the activity of osteoclasts but also that of osteoblasts. Namely, the coupling process between osteoclasts and osteoblasts could be disturbed by osteoclast apoptosis[43].

Additionally, bisphosphonates impair osteoblast activation[44], likely affecting spatial distribution, where cells are less guided by the mechanical signal.

Regions with high local strain are linked to higher occurrences of microscopic tissue damage[45] of which even small amounts can cause large reductions in strength[46] and increase fatigue fracture risk[47]. Cosman et al.[48] reported a decrease in vertebral fractures after monthly sclerostin antibody treatment in postmenopausal women, where fatigue fractures are common[49], but not in other bones. Increases in mechanoregulation induced by sclerostin antibody treatment might also help decrease fatigue fracture risk.

As a limitation, our developed system does not yet incorporate the level of the transcriptome[50]. While our results highlight the promise of mechanical loading is as adjunct to anabolic therapies, clinical studies will be required to determine through which specific types of physical activity this can be translated to humans. Similar to finding a suitable dose regimen for pharmaceuticals, optimizing specific exercise protocols is essential given that treatment outcomes depend on the type of exercise performed.

In conclusion, the current study revealed that drug treatments target trabecular bone (re)modeling to the mechano-functionally relevant places, and anabolic drug treatment in combination with mechanical loading synergistically increased the bone response. The synergistic increases extended across trabecular strength and mechanoregulation at the tissue level and can be explained by shifts in the (re)modeling thresholds as described by Frost in the mechanostat more than 30 years ago.

Being able to link organ-level changes induced by physical or pharmaceutical therapies to the mechanosensitivity of the cells provides information on how well bones and tissues under pathological or treatment conditions can adapt the skeleton to mechanical demands, a task for which the body has optimized itself for millions of years of evolution. Load-bearing physical

activity may represent a promising adjunct option for osteoporosis patients on anabolic osteoporosis therapy who are still physically active.

Methods

Study design

The study design is illustrated in Fig. 1a. In total, 120 female 15-week-old C57BL/6 mice (n=60, C57BL/JRccHsd, RCC/Harlan; Füllinsdorf, Switzerland/ Horst, The Netherlands; n=60, C57BL/6JRj mice (Janvier Labs, Le Genest-Saint-Isle, France) were subjected to bilateral ovariectomy. A basal micro-CT image of the 6th caudal vertebra was obtained (Scanco Medical, Brüttisellen, Switzerland). Recovery lasted five weeks after surgery, as in this period, an osteopenic state was established in the trabecular compartment of the 6th caudal vertebra in a previous study[51]. Pinning of the adjacent vertebrae as preparation for the loading procedure took place in week 17. At week 20, the animals were divided into 8 groups and the following treatments were administered for the following four weeks: BIS (n=9), BIS + ML (n=9), PTH (n=10), PTH + ML (n=9), SclAB (n=9), SclAB + ML (n=8), ML (n=26), VEH (n=25). 10 mice were excluded due to swollen tails or loose pins. In the SclAB study, 4 mice showed a periosteal reaction, possibly due to injury of the periosteum during intravenous injection at the tail vein. One mouse in the BIS + ML group did not lose bone volume after ovariectomy. These mice were excluded from evaluation, resulting in 105 animals included. Micro-CT was performed in weeks 15, 20, 22 and 24. Surgeries, imaging, and loading were performed under isoflurane anesthesia (induction 4%, maintenance 1.5-2.5%, Attane, Piramal Healthcare, India). Vehicle control was an isotonic buffer (pH 5.3). While the data was gained in four experiments (at different times), study and loading parameters were not different except for the administered pharmaceutical treatments, thus combined in this study. The bone responses of the VEH and

the ML groups of both mouse lines (JRccHsd and 6JRj) showed no differences in reactions ($\Delta BV/TV_{w20-24;}$ VEH: $p = 0.937$; ML: $p = 0.206$; two-way ANOVA with Tukey post-hoc test), thus ML groups from all experiments and VEH groups from all experiments were merged, explaining the larger sample size in these groups. All animal experiments were performed with approval of the local authority (Kantonales Veterinäramt Zürich, Zurich, Switzerland).

Mechanical loading

To induce a bone response under controlled loading conditions, we used an *in vivo* mouse tail loading model of trabecular bone adaptation[51-53]. Three weeks before loading start, pins were inserted into the 5th and 7th caudal vertebra under fluoroscopic control. At loading start, the 6th caudal vertebra (CV6) was subjected to cyclic mechanical loading at a force of 8N (or 0N sham loading) delivered through a specifically designed CVAD loading device, 3 times/week for 4 weeks at 10 Hz and 3000 cycles.

Pharmaceutical treatment

The BIS group received 100 µg/kg zoledronate (Zometa 4 mg/5 ml; Novartis Pharma Schweiz AG, Bern) subcutaneously once in week 20. Corresponding VEH (0.9% NaCl, B. Braun Medical AG, Switzerland) was injected at the same time point. Mice in the PTH study received 40 µg/kg PTH (hPTH 1-34, Bachem AG, Switzerland) or the according VEH (0.9% NaCl) subcutaneously daily over four weeks. SclAB (100 mg/kg, Novartis Pharma AG, Basel, Switzerland) or the corresponding VEH (isotonic buffer, pH 5.3) was injected weekly over 4 weeks.

Bone morphometry

Micro-CT images were obtained with a vivaCT 40 (Scanco Medical AG, Brüttisellen, Switzerland) operated at 55 kVp and 146 µA. 1000 projection images were obtained with an integration time of 200 ms. Grayscale images were reconstructed using a Feldkamp algorithm, with automated beam hardening correction, resulting in an isotropic voxel size of 10.5 µm. The image of week 20 was aligned in the main loading direction. Follow up scans were registered to the previous scan. A constrained 3D Gauss filter (sigma 1.2, support 1) and a global thresholding procedure (580 mgHA/cm^3) were applied. Automated masks were created to extract the trabecular bone volumes (trabecular mask truncated by 10% of length at both ends to exclude epiphyses and primary spongiosa; middle 26% removed because this area is almost void of trabeculae)[18]. The cortical mask included 75% of the length of the inner mask[18]. Static trabecular bone morphometric parameters were calculated according to Bouxsein et al.[54]. Dynamic bone morphometry was performed by registering and superimposing segmented bone volume images of consecutive time points. Bone formation and resorption rates were calculated as described previously[55] over two two-week periods (20-22 and 22-24).

Finite element analysis of mechanical properties

Finite-element simulations were used to analyze mechanical properties of the vertebrae. 3D micro-FE models were generated by converting all voxels of the micro-CT image to 8 node hexahedral elements, with each model consisting of approximately 1.8 million elements. A Young's modulus of 14.8 GPa and a Poisson's ratio of 0.3[52] were assigned. Each model was solved with ParOSol[56] running on the Euler cluster operated by Scientific IT Services at ETH Zurich. Cylindric intervertebral disks (10% of absolute height) were applied and assigned the same Young's modulus and Poisson's ratio as bone. The top of the model was displaced by 1% of the total vertebral length, while the bottom was fixed. The resulting reaction force was rescaled to the value of the force applied in the experimental setup; consequently, all the FE

outcomes were rescaled accordingly (4 N for non-loaded[57] and 8 N for loaded mice). Strain energy density (SED), defined as the increase in energy associated with the tissue deformation per unit volume, and effective strain were used as the mechanical signal. Trabecular bone strength was estimated for each mouse at each time point by using the Pistoia criterion[58] which assumes that bone failure is initiated if a certain percentage of the bone tissue (2%) is strained beyond the tissue yield effective strain (7000 $\mu\varepsilon$). For the trabecular bone strength estimation, the full bone was modeled but only the effective strains in the trabecular compartment were analyzed.

Local mechanoregulation analysis

To associate sites of formation or resorption with the local mechanical environment on the trabecular bone surface, the mechanical environment at week 20 was projected into the volumetric formation and resorption clusters from week 20 to 22 using the method published by Griesbach et al.[17]. The two volumetric clusters for formation and resorption as well as the quiescent surface of the superimposed micro-CT scans were used as masks and applied to the SED image. Mean SED values from these clusters were calculated and normalized by mean quiescent SED of each group[10]. Area under the curve for the receiver operating characteristic were calculated for formation (AUC_F) and resorption (AUC_R) based on the respective clustered mechanical values and the mechanical values on the bone surface[17, 53].

Conditional probabilities for each (re)modeling event were calculated by creating histograms of SED values with 50 bins for formed, quiescent and resorbed bone volumes, rescaling them to contain the same amount of values to remove dependencies on imbalances in the (re)modeling process due to differences between animals or treatments, and consequently dividing the rescaled histograms bin-wise by the sum of the three (re)modeling histograms[10].

Mean conditional probabilities were calculated for all animals within one group and fitted with exponential functions. To compare parameters extracted from these functions, a bootstrapping approach was used by creating 2500 subsamples from each group[16, 59], fitting the conditional probability functions to the mean curve of each subsample. For formation and resorption, the minimum probability, indicating the amount of non-targeted formation or resorption, was compared between groups. Additionally, the intersections between the resorption and quiescent curve (RQ), and the quiescent and formation curve (QF) were computed. Furthermore, CCR values were calculated from the mean conditional probabilities from all animals, returning a scalar value between 0.33 and 1 assessing overall mechanoregulation, with 0.33 meaning (re)modeling is independent of the mechanical signal and 1 meaning it is entirely dependent on the mechanical signal.

(Re)modeling velocities (RmVs) and their mechanostat parameters were calculated according to Marques et al. for each animal[16]. As treatments altered the curve characteristics (Fig. 7), we extended the hyperbolic curve fit used by Marques et al. by adding a linear component $RmV(x) = y_0 - \frac{a}{b*x} + c * x$ and fitted it to the mean RmV curve for each group. Minimum and maximum RmV, as well as (re)modeling thresholds (RmTs) were extracted from the resulting curve. To enable statistical comparison of parameters derived from the curve fits, we used a bootstrapping approach creating 2500 subsamples from each group and fitting the extended hyperbolic function to the mean RmV curve of each subsample[16, 59]. To compare treatment effects, we subtracted each RmV curve with the control RmV curve for the VEH group. The result represented the respective treatment effect on the RmV over the relevant effective strain values for each group. Additionally, we added the treatment effect of each pharmaceutical treatment to the effect of the ML group, to use as a reference of comparison for the combined treatment and assess and visualize if the effect was additive or even synergistic[34].

Statistical methods

Morphometric parameters were normalized to treatment start (week 20) for each animal. For the effect of ovariectomy, statistical analysis was performed using one-way ANOVA. Static, dynamic, and mechanical treatment effects were compared using two-way ANOVA over time and group with Tukey post-hoc-test or Kruskal-Wallis with Bonferroni correction after testing for normality.

Comparison of parameters of the mechanoregulation analysis was performed using Kruskal-Wallis-Test with Tukey post-hoc test. Correlations were assessed with Pearson's coefficient and R^2. Synergism was defined as when the combined treatment exceeded the sum of the two single treatments. Additivity was defined as when the combined treatment was equal to the sum of the two single treatments where E represents the effect:

- **Synergism S:** The combined effect of two drugs is greater than the sum of their individual effects: $E_{comb} > E_{drug1} + E_{drug2}$.
- **Additivity A:** The combined effect of two drugs equals the sum of their individual effects: $E_{comb} = E_{drug1} + E_{drug2}$. A 10% above above and below equality was allowed.
- **Interference I:** The combined effect of two drugs is less than the sum of their individual effects E, indicating interference (I) between the drugs: $E_{comb} < E_{drug1} + E_{drug2}$.

Statistical analysis was performed using R (R, Auckland, New Zealand[60]) and GraphPad Prism 10 (GraphPad software, Boston, United States). Data are presented as mean ± standard deviation unless otherwise specified. P-values lower than 0.05 are considered significant.

Acknowledgments

We acknowledge Kathleen Koch for assistance and performance of animal experiments of the PTH and BIS groups, and Dr. Ulrike Kettenberger for assistance and performance of animal experiments of the PTH group. This work was funded by the European Union grant VPHOP (FP7-ICT-2008-223865) and the European Research Council ERC Advanced grant (MechAGE ERC-2016-ADG-741883).

Author contributions

RM, GAK, PJR designed the experiment. CW, GAK, MS, FML performed the experiment. JG, FAS, CW, MS, FML, GAK, FCM performed image processing. MK provided pharmaceutical agents. RM, GAK, PJR supervised the project. FAS and JG wrote the original draft of the manuscript. All authors were involved in discussions during the work and in the preparation of the manuscript.

Competing interests

M.K. and P.R. are employees of Novartis. The other authors declare they have no competing interests.

Data availability

The main data supporting the findings of this study are available within the paper. The raw data generated during the study are available for research purposes from the corresponding author on reasonable request.

References

1. Kanis, J.A. et al. A reference standard for the description of osteoporosis. *Bone* **42**, 467-475 (2008).
2. Dell, R.M. et al. Incidence of atypical nontraumatic diaphyseal fractures of the femur. *J Bone Miner Res* **27**, 2544-2550 (2012).
3. Baron, R. & Kneissel, M. WNT signaling in bone homeostasis and disease: from human mutations to treatments. *Nat Med* **19**, 179-192 (2013).
4. Ominsky, M.S., Boyce, R.W., Li, X. & Ke, H.Z. Effects of sclerostin antibodies in animal models of osteoporosis. *Bone* **96**, 63-75 (2017).
5. Frost, H.M. The mechanostat: a proposed pathogenic mechanism of osteoporoses and the bone mass effects of mechanical and nonmechanical agents. *Bone Miner* **2**, 73-85 (1987).
6. Frost, H.M. Bone "mass" and the "mechanostat": a proposal. *Anat Rec* **219**, 1-9 (1987).
7. Frost, H.M. Bone's mechanostat: a 2003 update. *Anat Rec A Discov Mol Cell Evol Biol* **275**, 1081-1101 (2003).
8. Wolff, J. Das Gesetz der Transformation der Knochen (The Law of Bone Remodelling). *Berlin, Germany: Springer-Verlag* (1892).
9. Huiskes, R. If bone is the answer, then what is the question? *J Anat* **197**, 145-156 (2000).
10. Schulte, F.A. et al. Local mechanical stimuli regulate bone formation and resorption in mice at the tissue level. *PLoS One* **8**, e62172 (2013).
11. Razi, H. et al. Aging Leads to a Dysregulation in Mechanically Driven Bone Formation and Resorption. *J Bone Miner Res* **30**, 1864-1873 (2015).
12. Christen, P. et al. Bone remodelling in humans is load-driven but not lazy. *Nat Commun* **5**, 4855 (2014).
13. Walle, M. et al. Bone Mechanoregulation Allows Subject-Specific Load Estimation Based on Time-Lapsed Micro-CT and HR-pQCT in Vivo. *Front Bioeng Biotechnol* **9**, 677985 (2021).
14. Burr, D.B. Targeted and nontargeted remodeling. *Bone* **30**, 2-4 (2002).
15. Graham, J.M., Ayati, B.P., Holstein, S.A. & Martin, J.A. The role of osteocytes in targeted bone remodeling: a mathematical model. *PLoS One* **8**, e63884 (2013).
16. Marques, F.C. et al. Mechanostat parameters estimated from time-lapsed micro-computed tomography data of mechanically driven bone adaptation are logarithmically dependent on loading frequency. *Front Bioeng Biotech* **11** (2023).
17. Griesbach, J.K., Schulte, F.A., Schadli, G.N., Rubert, M. & Muller, R. Mechanoregulation analysis of bone formation in tissue engineered constructs requires a volumetric method using time-lapsed micro-computed tomography. *Acta Biomater* (2024).
18. Lambers, F.M., Schulte, F.A., Kuhn, G., Webster, D.J. & Muller, R. Mouse tail vertebrae adapt to cyclic mechanical loading by increasing bone formation rate and decreasing bone resorption rate as shown by time-lapsed in vivo imaging of dynamic bone morphometry. *Bone* **49**, 1340-1350 (2011).
19. Taylor, S. et al. Time-dependent cellular and transcriptional changes in the osteoblast lineage associated with sclerostin antibody treatment in ovariectomized rats. *Bone* **84**, 148-159 (2016).
20. Ominsky, M.S. et al. Romosozumab Improves Bone Mass and Strength While Maintaining Bone Quality in Ovariectomized Cynomolgus Monkeys. *Journal of Bone and Mineral Research* **32**, 788-801 (2017).
21. Morse, A. et al. Sclerostin Antibody Augments the Anabolic Bone Formation Response in a Mouse Model of Mechanical Tibial Loading. *J Bone Miner Res* **33**, 486-498 (2018).
22. Eriksen, E.F. et al. Modeling-Based Bone Formation After 2 Months of Romosozumab Treatment: Results From the FRAME Clinical Trial. *J Bone Miner Res* **37**, 36-40 (2022).
23. Morse, A. et al. Mechanical load increases in bone formation via a sclerostin-independent pathway. *J Bone Miner Res* **29**, 2456-2467 (2014).
24. Witcher, P.C. et al. Sclerostin neutralization unleashes the osteoanabolic effects of Dkk1 inhibition. *Jci Insight* **3** (2018).

25. Morse, A. et al. KO Mice Treated with Sclerostin Antibody Have Additional Increases in Bone Volume. *Calcified Tissue Int* **103**, 298-310 (2018).
26. Florio, M. et al. A bispecific antibody targeting sclerostin and DKK-1 promotes bone mass accrual and fracture repair. *Nature Communications* **7** (2016).
27. Choi, J.U.A., Kijas, A.W., Lauko, J. & Rowan, A.E. The Mechanosensory Role of Osteocytes and Implications for Bone Health and Disease States. *Front Cell Dev Biol* **9** (2022).
28. Baertschi, S., Baur, N., Lueders-Lefevre, V., Voshol, J. & Keller, H. Class I and IIa Histone Deacetylases Have Opposite Effects on Sclerostin Gene Regulation. *J Biol Chem* **289**, 24995-25009 (2014).
29. Wein, M.N. et al. HDAC5 controls MEF2C-driven sclerostin expression in osteocytes. *J Bone Miner Res* **30**, 400-411 (2015).
30. Robling, A.G. et al. Mechanical stimulation of bone in vivo reduces osteocyte expression of Sost/sclerostin. *J Biol Chem* **283**, 5866-5875 (2008).
31. Chen, S. et al. Structural and functional studies of LRP6 ectodomain reveal a platform for Wnt signaling. *Dev Cell* **21**, 848-861 (2011).
32. Ryder, K.D. & Duncan, R.L. Parathyroid hormone modulates the response of osteoblast-like cells to mechanical stimulation. *Calcif Tissue Int* **67**, 241-246 (2000).
33. Hagino, H., Okano, T., Akhter, M.P., Enokida, M. & Teshima, R. Effect of parathyroid hormone on cortical bone response to in vivo external loading of the rat tibia. *J Bone Miner Metab* **19**, 244-250 (2001).
34. Miller, C.J. et al. Cortical thickness adaptation to combined mechanical loading and parathyroid hormone treatments is site specific and synergistic in the mouse tibia model. *Bone* **180**, 116994 (2024).
35. Sugiyama, T. et al. Mechanical loading enhances the anabolic effects of intermittent parathyroid hormone (1-34) on trabecular and cortical bone in mice. *Bone* **43**, 238-248 (2008).
36. Meakin, L.B. et al. Parathyroid hormone's enhancement of bones' osteogenic response to loading is affected by ageing in a dose- and time-dependent manner. *Bone* **98**, 59-67 (2017).
37. Robinson, S.T., Shyu, P.T. & Guo, X.E. Mechanical loading and parathyroid hormone effects and synergism in bone vary by site and modeling/remodeling regime. *Bone* **153**, 116171 (2021).
38. Uusi-Rasi, K. et al. Effect of alendronate and exercise on bone and physical performance of postmenopausal women: a randomized controlled trial. *Bone* **33**, 132-143 (2003).
39. Chilibeck, P.D. et al. The effect of strength training combined with bisphosphonate (etidronate) therapy on bone mineral, lean tissue, and fat mass in postmenopausal women. *Can J Physiol Pharmacol* **80**, 941-950 (2002).
40. Kistler-Fischbacher, M., Yong, J.S., Weeks, B.K. & Beck, B.R. A Comparison of Bone-Targeted Exercise With and Without Antiresorptive Bone Medication to Reduce Indices of Fracture Risk in Postmenopausal Women With Low Bone Mass: The MEDEX-OP Randomized Controlled Trial. *J Bone Miner Res* **36**, 1680-1693 (2021).
41. Stadelmann, V.A., Bonnet, N. & Pioletti, D.P. Combined effects of zoledronate and mechanical stimulation on bone adaptation in an axially loaded mouse tibia. *Clin Biomech (Bristol, Avon)* **26**, 101-105 (2011).
42. Sugiyama, T. et al. Risedronate does not reduce mechanical loading-related increases in cortical and trabecular bone mass in mice. *Bone* **49**, 133-139 (2011).
43. Sims, N.A. & Martin, T.J. Osteoclasts Provide Coupling Signals to Osteoblast Lineage Cells Through Multiple Mechanisms. *Annu Rev Physiol* **82**, 507-529 (2020).
44. Jensen, P.R., Andersen, T.L., Chavassieux, P., Roux, J.P. & Delaisse, J.M. Bisphosphonates impair the onset of bone formation at remodeling sites. *Bone* **145** (2021).
45. Acevedo, C., Stadelmann, V.A., Pioletti, D.P., Alliston, T. & Ritchie, R.O. Fatigue as the missing link between bone fragility and fracture. *Nat Biomed Eng* **2**, 62-71 (2018).
46. Hernandez, C.J., Lambers, F.M., Widjaja, J., Chapa, C. & Rimnac, C.M. Quantitative relationships between microdamage and cancellous bone strength and stiffness. *Bone* **66**, 205-213 (2014).
47. Lambers, F.M., Bouman, A.R., Rimnac, C.M. & Hernandez, C.J. Microdamage caused by fatigue loading in human cancellous bone: relationship to reductions in bone biomechanical performance. *PLoS One* **8**, e83662 (2013).

48. Cosman, F. et al. Romosozumab Treatment in Postmenopausal Women with Osteoporosis. *N Engl J Med* **375**, 1532-1543 (2016).
49. Keaveny, T.M., Wachtel, E.F. & Kopperdahl, D.L. Mechanical behavior of human trabecular bone after overloading. *J Orthop Res* **17**, 346-353 (1999).
50. Mathavan, N. et al. Spatial transcriptomics in bone mechanomics: Exploring the mechanoregulation of fracture healing in the era of spatial omics. *Sci Adv* **11**, eadp8496 (2025).
51. Lambers, F.M., Kuhn, G., Schulte, F.A., Koch, K. & Muller, R. Longitudinal assessment of in vivo bone dynamics in a mouse tail model of postmenopausal osteoporosis. *Calcif Tissue Int* **90**, 108-119 (2012).
52. Webster, D.J., Morley, P.L., van Lenthe, G.H. & Muller, R. A novel in vivo mouse model for mechanically stimulated bone adaptation--a combined experimental and computational validation study. *Comput Methods Biomech Biomed Engin* **11**, 435-441 (2008).
53. Scheuren, A.C. et al. Mechano-Regulation of Trabecular Bone Adaptation Is Controlled by the Local in vivo Environment and Logarithmically Dependent on Loading Frequency. *Front Bioeng Biotechnol* **8**, 566346 (2020).
54. Bouxsein, M.L. et al. Guidelines for Assessment of Bone Microstructure in Rodents Using Micro-Computed Tomography. *Journal of Bone and Mineral Research* **25**, 1468-1486 (2010).
55. Schulte, F.A., Lambers, F.M., Kuhn, G. & Muller, R. In vivo micro-computed tomography allows direct three-dimensional quantification of both bone formation and bone resorption parameters using time-lapsed imaging. *Bone* **48**, 433-442 (2011).
56. Flaig, C. & Arbenz, P. A scalable memory efficient multigrid solver for micro-finite element analyses based on CT images. *Parallel Comput* **37**, 846-854 (2011).
57. Christen, P., van Rietbergen, B., Lambers, F.M., Muller, R. & Ito, K. Bone morphology allows estimation of loading history in a murine model of bone adaptation. *Biomech Model Mechanobiol* **11**, 483-492 (2012).
58. Pistoia, W. et al. Estimation of distal radius failure load with micro-finite element analysis models based on three-dimensional peripheral quantitative computed tomography images. *Bone* **30**, 842-848 (2002).
59. Davison, A.C., Hinkley, D.V. & Schechtman, E. Efficient Bootstrap Simulation. *Biometrika* **73**, 555-566 (1986).
60. Team, R.D.C. in R Foundation for Statistical Computing (Vienna, Austria; 2007).